Nano Research
2020, 13(2): 551–556
ISSN 1998-0124 CN 11-5974/O4
https://doi.org/10.1007/s12274-020-2650-y

Research Article

Synergetic catalysis enhancement between H_2O_2 and TiO_2 with single-electron-trapped oxygen vacancy

Zhijiao Wu[1,§], Kai Guo[1,4,§], Shuang Cao[1] (✉), Wenqing Yao[3] (✉), and Lingyu Piao[1,2] (✉)

[1] *CAS Key Laboratory of Standardization and Measurement for Nanotechnology, CAS Center for Excellence in Nanoscience, National Center for Nanoscience and Technology, Beijing 100190, China*
[2] *Center of Materials Science and Optoelectronics Engineering, University of Chinese Academy of Sciences, Beijing 100049, China*
[3] *Department of Chemistry, Tsinghua University, Beijing 100084, China*
[4] *University of Chinese Academy of Sciences, Beijing 100049, China*
[§] *Zhijiao Wu and Kai Guo contributed equally to this work.*

Received: 4 November 2019 / **Revised:** 27 December 2019 / **Accepted:** 8 January 2020

ABSTRACT

The TiO_2-H_2O_2 system possesses excellent oxidation activity even under dark conditions. However, the mechanism of this process is unclear and inconsistent. In this work, the binary component system containing TiO_2 nanoparticles (NPs) with single electron-trapped oxygen vacancy (SETOV, $V_O\cdot$) and H_2O_2 exhibit excellent oxidative performance for tetracycline, RhB, and MO even without light irradiation. We systematically investigated the mechanism for the high activity of the TiO_2-H_2O_2 under dark condition. Reactive oxygen species (ROS) induced from H_2O_2 play a significant role in improving the catalytic degradation activities. X-ray photoelectron spectroscopy (XPS) and electron paramagnetic resonance (EPR) results firstly confirm that H_2O_2 is primarily activated by SETOVs derived from the TiO_2 NPs through direct contribution of electrons, producing both $\cdot O_2^-$/$\cdot$OOH and $\cdot$OH, which are responsible for the excellent reactivity of TiO_2-H_2O_2 system. This work not only provides a new perspective on the role of SETOVs playing in the H_2O_2 activation process, but also expands the application of TiO_2 in environmental conservation.

KEYWORDS

single-electron-trapped oxygen vacancy, TiO_2 nanoparticle, H_2O_2, dark reaction, superoxide radicals, hydroxyl radical

1 Introduction

Photocatalytic oxidation is regarded as a promising strategy for pollutant removal in water [1–6]. Titanium dioxide (TiO_2), one of the best-known semiconductor photocatalysts, is identified as a promising pollutants removing material due to its evidently photocatalytic oxidation ability [1–13]. However, TiO_2 is a type of wide bandgap semiconductor (3.2 eV) and it only adsorbs ultraviolet light, which greatly limits its practical applications. Most recently, the addition of H_2O_2 has been proved to efficiently promote catalytic activity of TiO_2 even without any light irradiation, which may potentially overcome the limitation of light irradiation and therefore expand the application of TiO_2 in environmental conservation [14–19].

According to most recent findings, the enhanced oxidative behavior of TiO_2-H_2O_2 system has been ascribed to the H_2O_2 activation by TiO_2, which induces the generation of reactive oxygen species (ROS) including $\cdot$OH and $\cdot O_2^-$/$\cdot$OOH on the surface of catalyst [14–18]. As we all know, both $\cdot$OH and $\cdot O_2^-$/$\cdot$OOH exhibit strong oxidative ability that can degrade organic dye molecules in water. However, the mechanisms of H_2O_2 activation and the role of ROS in the enhanced oxidation ability of TiO_2-H_2O_2 system are still controversial. For example, Zhang et al. demonstrated that H_2O_2 accepted electrons from surface Ti^{3+} and was activated into $\cdot$OH and $\cdot O_2^-$/$\cdot$OOH. The $\cdot$OH was confirmed to respond for the improved performance of TiO_2-H_2O_2 [17]. However, Wiedmer [18] put forward the viewpoint that only the $\cdot O_2^-$/$\cdot$OOH plays key role in enhancing performance of TiO_2-H_2O_2 rather than $\cdot$OH. Moreover, the mechanism of transferring H_2O_2 into $\cdot O_2^-$/$\cdot$OOH and $\cdot$OH by TiO_2 NPs has not been studied. In order to provide more accurate information for constructing highly efficient TiO_2-H_2O_2 system, more work should be focused on the mechanism of H_2O_2 activation by TiO_2 as well as the role of ROS.

Single electron-trapped oxygen vacancy in TiO_2 bulk phase (SETOV, $V_O\cdot$), a typical intrinsic defect, was demonstrated to affect TiO_2 photocatalytic performance via electronic interaction [20]. Thus, it is significant to study whether the H_2O_2 can be effectively activated by SETOV into ROS through electronic interaction and consequentially improve the oxidative ability of TiO_2-H_2O_2 in dark. However, SETOV in TiO_2 bulk has rarely been investigated for H_2O_2 activation in dark and the related catalytic mechanism for TiO_2-H_2O_2 remains unclear.

In our work, TiO_2 NPs with SETOVs in bulk were prepared and then mixed with H_2O_2 to form TiO_2-H_2O_2 system. The degradation ability of TiO_2-H_2O_2 for tetracycline, RhB, and MO in dark is greatly enhanced. The catalytic efficiencies are more than 2 and 1.5 times higher than the reported highest value for RhB and MO degradation, respectively. Here, we provide a fundamental mechanism of activating H_2O_2 into ROS by SETOVs, which can provide key information on H_2O_2 activation as well as promote practical application of TiO_2 greatly.

Address correspondence to Shuang Cao, caos@nanoctr.cn; Wenqing Yao,yaowq@tsinghua.edu.cn; Lingyu Piao, piaoly@nanoctr.cn

TSINGHUA UNIVERSITY PRESS Springer

2 Experimental

2.1 Synthesis of TiO_2 nanoparticles with different contents of SETOVs

Titanium tetrachloride ($TiCl_4$) was used as the precursor for the obtained TiO_2 NPs. A 0.02 mol/L $TiCl_4$ solution was firstly prepared by slowly adding $TiCl_4$ into ice water under stirring and then dropped into 50 mL 0.5 mol/L ammonia with 65 drops per minute under 200 rpm stirring at room temperature until the pH value of the solution reached ~ 8. A white precipitate was obtained and washed with distilled water by centrifugation until chloride ions were not detectable in the washed water (1.0 wt.% $AgNO_3$ solution). Different amounts of precipitation were dispersed in 50 mL anhydrous ethyl alcohol by ultrasonic treatment for 20 min in autoclave and kept at 150 °C for 3 h (shown in Table 1). The obtained products were dispersed by ultrasonic for 20 min directly to form a stable sol system. Three kinds of TiO_2 NPs and their related suspension after adding H_2O_2 were marked as A1, A2 and A3. 1.5 mL of H_2O_2 (30 wt.%) were added into different volumes of the obtained sol and stirred for 30 min (shown in Table 1). The color of the sol turned to pale yellow. In order to obtain suspension with 0.05 g/L TiO_2, ~ 450 mL deionized water was added. The final concentration of H_2O_2 in suspension is 29 mM. Three kinds of TiO_2 NPs after adding H_2O_2 were marked as S1, S2 and S3, respectively.

2.2 Catalysis experiment

The reactivity of TiO_2-H_2O_2 sample was evaluated by the degradation of RhB, methyl orange (MO) and tetracycline in cylindrical quartz flask. For degradation of RhB, reaction solutions were obtained by adding 0.5 mL 500 mg·L^{-1} RhB solution into 100 mL of 0.05 g·L^{-1} TiO_2 suspension containing 29 mM H_2O_2. For degradation of MO, reaction solutions were obtained by adding 1.0 mL 500 mg·L^{-1} MO solution into 99 mL of 0.05 g·L^{-1} TiO_2 suspension containing 29 mM H_2O_2. For degradation of tetracycline, reaction solution was obtained by adding 1 mg tetracycline into 99 mL of 0.05 g·L^{-1} TiO_2 suspension containing 29 mM H_2O_2. At intervals, 3 mL of solution was taken out every 15 minutes for RhB, 30 min for MO, and 4 h for tetracycline. The solution was centrifuged at 10,000 rpm for 3 min to remove the solid catalysts. The ultraviolet–visible (UV–vis) absorption spectra of the RhB, MO, and tetracycline were recorded from the absorbance at 553, 464, and 359 nm, respectively. For cyclic tests, H_2O_2 and RhB solution were added into the suspension after each run. The concentrations of H_2O_2 and RhB were 29 mM and 2.5 mg·L^{-1} for each run. Fluorescence (FL) absorption spectra were using terephthalate (TANa) (5×10^{-3} M) which reacted with ·OH to produce highly fluorescent 2-hydroxyterephthalic acid (TAOH), TAOH emits fluorescence at around 425 nm upon excitation of its 312 nm absorption band. Tests were performed in 3.0 mL of solution at pH = 6 for 10 min; then centrifuged to remove catalyst and put the solution into quartz cell.

2.3 Characterization

The morphologies of the TiO_2 samples were determined by transmission electron microscopy (TEM, Tecnai G2 F20 U-TWIN). For TEM observation, the samples were dispersed in ethanol by ultrasonic treatment for 5 min and dropped onto carbon-coated copper grids. The crystalline structures of the samples were analyzed using X-ray diffractometer on a Smartlab (9) with Cu Kα radiation, and the spectra were recorded in the 2θ range of 20°–80° at a rate of 8°·min^{-1} and step size of 0.02°. The TiO_2 powders were pressed into a quartz cell. Raman spectrum analysis was conducted on a Renishaw Invia plus spectrometer operating at 633 nm. X-ray photoelectron spectroscopy (XPS, Escalab 250Xi) was performed using Al Kα X-rays ($h\nu$ = 1,486.6 eV), hybrid (magnetic/electrostatic) optics and a multi-channel plate and delay line detector. All XPS spectra were recorded using an aperture slot of 500 μm × 500 μm. High-resolution spectra were recorded with pass energy of 30 eV. The intensity of the XPS spectra has not been normalized. Au signal was used as a reference signal, and "shirly" model was employed to correct the XPS spectra. All the binding energies were calibrated by the C1s speak at 284.8 eV of the surface adventitious carbon. Nitrogen adsorption–desorption isotherms were collected on a NOVA3200e (Quantachrome Instruments) at 77 K. Before measurement, the samples were degassed at 473 K for 5 h. The electron paramagnetic resonance (EPR) spectra were recorded on a Bruker E 500 spectrometer at ambient temperature in the dark. The weight of all TiO_2 samples used to measure SETOVs was 20 mg. The samples used to measure ROS were prepared as follows. 3 mL of undiluted stable sol was mixed with 150 μL H_2O_2 (30 wt.%) for 30 min. 50 μL of this suspension was taken and introduced to 400 mM 5,5'-dimethyl-1-pirroline-N-oxide (DMPO) of the same volume. All the processes above are carried out in the absence of light. The evolved O_2 in the gas phase was examined by a Techcomp gas chromatography (GC-7900) with a thermal conductivity detector (TCD), 5 Å molecular sieve columns and Ar carrier. The suspension was purged with argon flow for 30 min to remove dissolved air, and then stand still in the dark for 1.5 h. The static fluorescence spectral measurements were carried out with an F-4600 (Hitachi) spectrofluorometer.

Table 1 Reaction conditions of A1, A2, A3 and S1, S2, S3

TiO_2 sample	Suspension	Amounts of precipitation	Volume of sol (mL)	Volume of water (mL)
A1	S1	1/4	38	460.5
A2	S2	1/3	29	469.5
A3	S3	1/5	48	450.5

3 Results and discussion

3.1 Morphology and structural of TiO_2 nanoparticles

The morphology and crystal structure of TiO_2 samples were investigated by TEM, as shown in Figs. 1(a)–1(c). Both A1 and A2 are composed of uniform nanoparticles with average diameter of 17.3 ± 3.2 and 18.9 ± 3.4 nm, respectively, and a small amount of amorphous TiO_2. While A3 is mainly composed of amorphous TiO_2, and few crystalline nanoparticles with average diameter of 13.9 ± 3.5 nm are observed. The

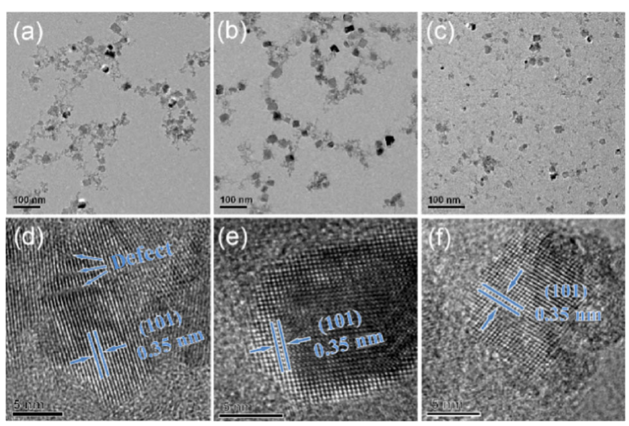

Figure 1 TEM images of TiO_2 samples: ((a) and (d)) A1, ((b) and (e)) A2, and ((c) and (f)) A3.

corresponding high-resolution TEM (HRTEM) images are shown in Figs. 1(d)–1(f). For A1, the lattice spacing of 0.35 nm is assigned to (101) facet, which is the thermodynamically stable crystal facet of anatase TiO_2 (Fig. 1(d)). Additionally, different distances co-exist in adjacent lattice planes are clearly observed, as marked with arrows in Fig. 1(d), indicating the existence of intrinsic bulk defects [21, 22]. A2 and A3 show continuous and ordered lattice fringes with lattice spacings of 0.35 nm, which correspond to the *d*-spacing of (101) plane of anatase TiO_2 [23]. Moreover, both A2 and A3 exhibit a relatively flat and smooth surface, further demonstrating the nanoparticles are mostly generated with few defects.

Phase structures of the obtained samples were investigated by X-ray diffraction (XRD). As shown in Fig. 2(a), diffraction peaks of the three samples match well with the standard peaks of anatase phase (JCPDS No.21−1272) [24–26]. The XRD pattern of A3 not only shows larger broad baseline, but also exhibits significantly lower peaks than that of A1 and A2. The result indicates the existence of amorphous phase and poor crystallinity of A3 sample [27].

The Raman spectra of samples contain four peaks in the range of 100–800 cm^{-1} (Fig. 2(b)). The most intense band at 146 cm^{-1} ($E_{g(1)}$ vibration mode) and three strong bands at 396 cm^{-1} ($B_{1g(1)}$), 517 cm^{-1} (A_{1g} + $B_{1g(2)}$) and 639 cm^{-1} ($E_{g(2)}$) are assigned to the characteristic vibrations of anatase TiO_2 [28–30], which are consistent with the XRD results. Besides, it should be noticed that the peaks of A3 are weak and broad with no obvious peak shift compared with A1 and A2. It is widely accepted that the broadening of Raman peaks is induced by the changes of particle size and presence of amorphous phase [31, 32]. Because the three samples possess very similar crystallite sizes, it can be concluded that the broadening peaks of A3 are induced by the presence of amorphous phases, further indicating its low crystallinity. The results are also consistent well with the analysis of XRD and TEM.

3.2 Catalytic activity

A1, A2 and A3 were mixed with H_2O_2 to form stable dispersions and marked with S1, S2 and S3, respectively. In order to investigate the catalytic activities, S1, S2 and S3 were evaluated by monitoring the decomposition of RhB, MO and tetracycline, respectively. Surprisingly, all the three dispersions exhibit catalytic activities toward RhB, MO, and tetracycline degradation without light irradiation (Fig. 3). Up to 90% of RhB can be degraded by S1 in 90 min (Fig. 3(a)), and the rate was over 2 times higher than reported values for the RhB degradation [19]. In addition, a ~ 80% removal of MO was achieved within 150 min in the S1 system (Fig. 3(b)), which was 1.5 times faster than the reported highest values [17]. Up to 70% of tetracycline can be degraded by S2 in 24 h (Fig. 3(c)), and the rate was over 1.3 times higher than reported values under same conditions [33]. Here the activity of S1 and S2 is very similar. These results indicate the excellent non-light-driven catalytic activity of S1. By contrast, the degradation ratios for S2 and S3 are 50% and 20% for RhB degradation, 50% and 15% for MO degradation within 90 and 150 min, respectively. Control experiments indicate that H_2O_2 or A1 alone show no degradation activity under the same condition, which confirm the existence of synergetic effect between TiO_2 and H_2O_2 [14–19]. The reusability of S1 was tested and the results were shown in Fig. 3(d). The catalytic activities were well maintained during five cyclic tests, indicating that the S1 was very stable during the catalysis.

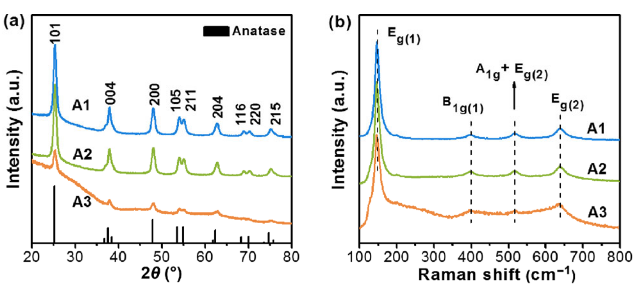

Figure 2 The XRD patterns (a) and Raman spectra (b) of TiO_2 samples.

3.3 Mechanism discussion

In general, surface property of catalyst plays an important role in the catalytic performance. In order to explain the positive synergetic effect, XPS analysis is performed to study the surface properties of TiO_2 samples (Fig. 4). In Ti 2p spectra (Fig. 4(a)), two major peaks at 458.7 and 464.5 eV are attributed to Ti^{4+} $2p_{3/2}$ and Ti^{4+} $2p_{1/2}$, respectively, indicating no Ti^{3+} species exist on the surface of the three samples. As shown in Figs. 4(b)–4(d), all samples exhibit a broad O 1s peak with a strong shoulder at a high binding energy, which can be deconvoluted into two peaks centered at 529.9 and 531.6 eV, which belong to the lattice oxygen (labeled as O_L) and surface oxygen forming Ti–OH (labeled as OH), respectively [34, 35]. The above results indicate that both Ti and oxygen species of all TiO_2 samples possess similar chemical nature. After adding H_2O_2, the Ti–OH can be translated to Ti–OOH. As shown in Fig. 4(e), another obvious peak at 532.9 eV belonging to Ti–OOH can be observed for A1 after adding H_2O_2 (S1). Besides, UV diffuse reflectance results demonstrate that the absorption band of A1 was at ~ 370 nm, while it extended to ~ 500 nm for S1 (Fig. 4(f)). It also can be observed by naked eyes and the color of the samples changed from white to yellow for Ti–OH and Ti–OOH, respectively [35]. Therefore, we can confirm that the –OOH groups of H_2O_2 would substitute for the –OH groups of Ti–OH, forming yellow Ti–OOH on the TiO_2 surface.

The XPS results also indicate that the obtained TiO_2 possesses abundant oxygen vacancy (the ratio of O_L/Ti is below 2), which provides active site for –OH adsorption (Fig. 4(g)). Generally, for the synthesis of TiO_2 with oxygen vacancy, the widely used methods are hydrogenation reduction [36], chemical reductant reduction [37] and high temperature oxygen deficient atmosphere reduction [38]. In our work, the TiO_2 with oxygen vacancy defects was synthesized by chemical reducing agent reduction method. Titanium chloride ($TiCl_4$) is used as Ti source and absolute ethanol as solvent, respectively. The ethanol provides a reductive environment to get TiO_2 with abundant oxygen

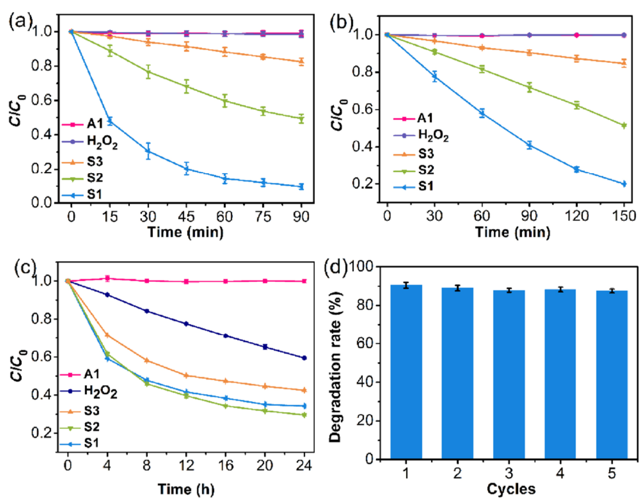

Figure 3 Degradation curves of (a) RhB, (b) MO, and (c) tetracycline solution without light irradiation using different TiO_2 suspensions. (d) Cyclic performance of S1 for degradation of RhB.

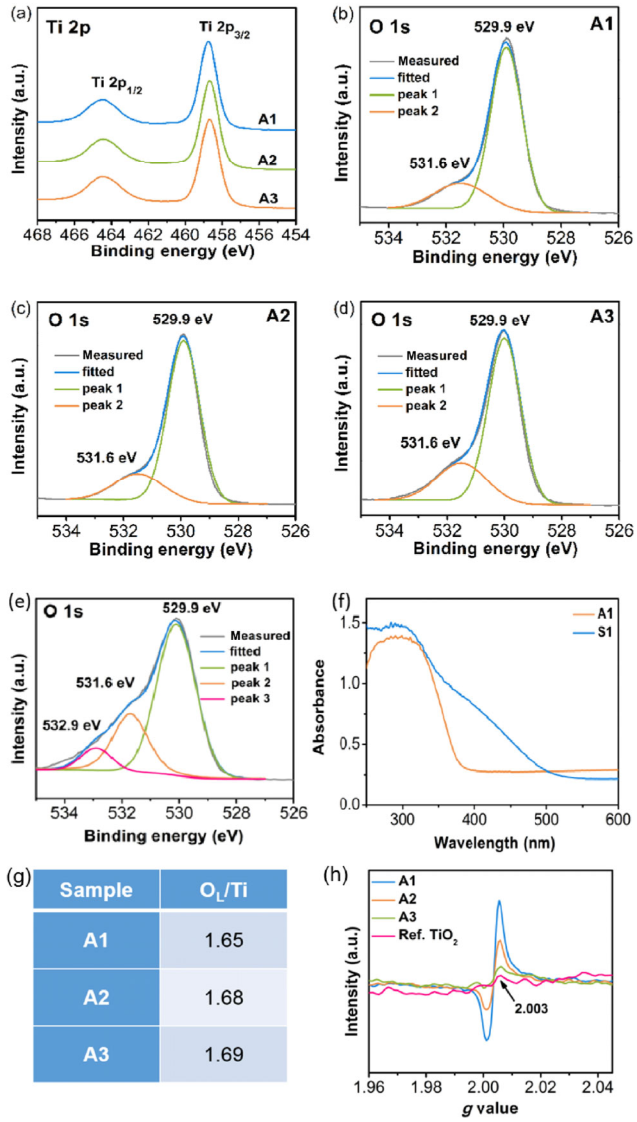

Sample	O_L/Ti
A1	1.65
A2	1.68
A3	1.69

Figure 4 XPS spectra of the TiO_2 samples (A1–A3): (a) Ti 2p spectra, (b)–(d) O 1s spectra. (e) XPS O1s spectra of the TiO_2-H_2O_2 samples. (f) UV visible diffuse reflectance spectrum spectra of A1 and S1. (g) Surface O/Ti ratios for all samples from XPS spectra. O_L: O 1s core level peak at ca. 529.9 eV for TiO_2. (h) EPR spectra of the TiO_2 samples recorded at 293 K in dark.

vacancy defects.

To explore the effect of oxygen vacancies or Ti^{3+} on the catalytic efficiency, EPR experiments are conducted at room temperature in the dark. As shown in Fig. 4(h), the *g*-values at 2.003 are observed which correspond to unpaired electrons trapped by oxygen vacancies in bulk, named SETOVs [20, 39, 40]. Obviously, A1 demonstrates a higher content of SETOVs than A2 and A3, which may lead to the much high reactivity. It has been reported that surface defects of Ti^{3+} could activate H_2O_2 in the dark [17]. However, no Ti^{3+} ($g \approx 1.94$) signal is observed in our sample. This result is consistent with the conclusion of XPS. Therefore, it can be reasoned that the SETOVs rather than Ti^{3+} plays a significant role in the catalytic process. BET results showed that A3 possesses the highest surface area (171.3 $m^2 \cdot g^{-1}$), followed by A1 (128.1 $m^2 \cdot g^{-1}$) and then A2 (123.9 $m^2 \cdot g^{-1}$). However, A3 demonstrated the lowest efficiency, which implies that the surface area is dispensable for activation ability of TiO_2 NPs.

In order to study the active species in the TiO_2-H_2O_2 system, EPR measurements using DMPO as the spin-trap reagent in the dark are firstly conducted. As shown in Fig. 5(a), no signals of active radicals for A1 and H_2O_2 are observed, explaining their non-catalytic ability in the dark. By contrast, six strong characteristic peaks ascribed to the DMPO spin adduct of $\cdot O_2^-$/$\cdot$OOH [18] are easily observed in the S1 without light irradiation. The result indicates the existence and essential role of $\cdot O_2^-$/$\cdot$OOH in degradation of organics. In addition, for the solid of S1(Fig. 5(b)), the obvious signals located at $g = 2.024$, $g = 2.008$, and $g = 2.002$ are the typical signals for $\cdot O_2^-$, further confirming the formation of Ti–OOH for A1 after adding H_2O_2 [14, 41, 42]. The signal intensity almost unchanged for A1-H_2O_2 after RhB degradation indicating the good stability. However, there is no obvious paramagnetic signal of $\cdot$OH detected in S1, which may be masked by the strong signal of $\cdot O_2^-$/$\cdot$OOH in the dark.

To verify the existence of $\cdot$OH in S1, we detect the $\cdot$OH in the dark reaction by the fluorescence probe of terephthalate (TANa). Under the condition of the existence of $\cdot$OH, TANa reacted with $\cdot$OH to form TAOH which emits strong fluorescence effect at 425 nm [43]. Figure 5(c) shows that when both TiO_2 and H_2O_2 exist, the intensity of fluorescence signal increases significantly than A1 or H_2O_2 alone. The results demonstrate that $\cdot$OH is another reactive intermediate during the reaction and control experiment results also indicate the $\cdot$OH is derived from the coexistence of both TiO_2 and H_2O_2. In addition, when isopropanol was introduced as the $\cdot$OH scavenger (Fig. 5(d)), the degradation rate of RhB was inhibited significantly from 90% to 78%. So, we can conclude that the $\cdot$OH is another reactive species in this system derived from TiO_2 and H_2O_2.

To further confirm the crucial role of SETOVs play during the catalytic process [44, 45], we introduced the control anatase sample with almost no oxygen vacancy (named ref

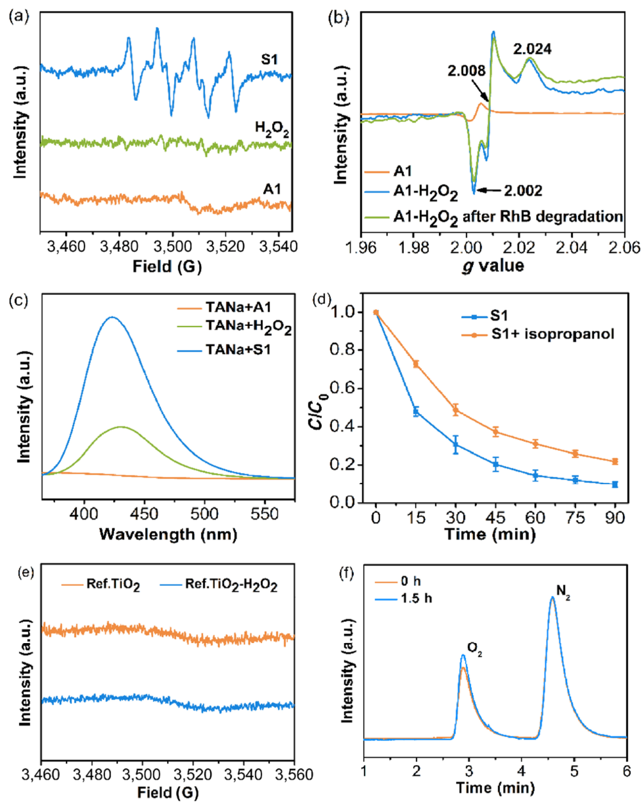

Figure 5 EPR spectra of (a) suspensions with different catalysts in dark after 60 s of reaction, and (b) A1 and A1-H_2O_2 before and after RhB degradation recorded at 293 K. (c) Degradation curves of RhB solution in S1 with and without isopropanol in dark. (d) FL spectrum of A1,H_2O_2 and S1 adding TANa; (e) EPR spectra of A1 and reference TiO_2 with no oxygen vacancy before and after adding H_2O_2. (f) GC curves of evolved O_2 in S1 after standing in the dark for 0 and 1.5 h.

TiO_2) as the reference to test the EPR signal before and after adding H_2O_2 using DMPO as capturing agent at room temperature. It was found that for ref TiO_2, there was almost no characteristic signal before and after adding H_2O_2, indicating the essential role of SETOVs for the formation of active species (Fig. 5(e)).

Based on the above results, we propose that the formation mechanism of ROS (such as $\cdot O_2^-$/·OOH and ·OH) was induced by SETOVs in TiO_2 bulk under non-light irradiation (Scheme 1 and Eqs. (1)–(6)). In the presence of H_2O_2, the –OOH groups of H_2O_2 would substitute for the –OH groups of Ti–OH, forming yellow surface complexes (Ti–OOH) represented as Eq. (1) as confirmed by XPS (Fig. 4(e)) and ultraviolet diffuse reflection results (Fig. 4(f)). The Ti–OOH reacts with an electron from the SETOVs to form the excited state (Ti–·OOH) which is highly active and tends to self-react to resume the original Ti-OH species in association with releasing O_2 [46], as described in Eqs. (2) and (3). The existence of Ti–·OOH has been confirmed by EPR results (Figs. 5(a) and 5(b)) and through a careful gas chromatography (GC) test, O_2 was successfully detected in S1 after standing in the dark for 90 min (Fig. 5(f)). As the chemical adsorption energy of O_2 molecule was efficiently reduced by SETOVs, as reported in Zeng's work [17], resulting in the easy adsorption of O_2 molecule onto TiO_2 surface. Subsequently, the $\cdot O_2^-$ radical is generated through the reduction of O_2 molecule by an electron from the SETOVs, as shown in Eq. (4), which have also been detected in EPR analysis (Figs. 5(a) and 5(b)). Meanwhile, the H_2O_2 in aqueous phase is activated by the electron from SETOVs, resulting in the production of ·OH radical (Eq. (5)) which is detected by fluorescence by using terephthalate (TANa) as probe (Fig. 5(c)) and isopropanol as trapping agent, respectively (Fig. 5(d)). Finally, H_2O_2 reacts with ·OH radical to form ·OOH radical [42, 47] (Eq. (6)), explaining the decreased rate of RhB degradation after adding the ·OH scavenger in S1. Both $\cdot O_2^-$/·OOH and ·OH possess strong oxidation ability and lead to the RhB and MO degradation in TiO_2-H_2O_2 system under non-light irradiation.

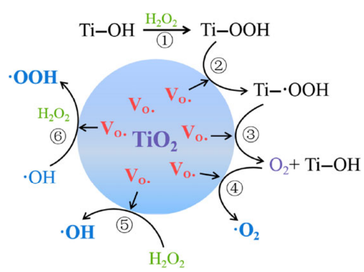

Scheme 1 Mechanism for the production of ROS in the dark. Vo·: the electron in SETOVs.

The above results confirmed that the $\cdot O_2^-$/·OOH and ·OH co-exist in non-irradiated TiO_2-H_2O_2 suspensions. It is the first time to demonstrate definitely that both $\cdot O_2^-$/·OOH and ·OH play essential role in the degradation of organics. Since the TiO_2 NPs are not irradiated and we can logically conclude that the e^-_{CB}-h^+_{VB} pair are not created. On the basis of EPR data, SETOVs in TiO_2 can trap single electron in the dark and the formation of $\cdot O_2^-$/·OOH and ·OH is the key factor.

$$\text{Ti–OH} + H_2O_2 \rightarrow \text{Ti–OOH} + H_2O \quad (1)$$

$$\text{Ti–OOH} + V_O\cdot \rightarrow \text{Ti–·OOH} \quad (2)$$

$$\text{Ti–·OOH} + V_O\cdot \rightarrow 1/2\ O_2 + \text{Ti–OH} \quad (3)$$

$$O_2 + V_O\cdot \rightarrow \cdot O_2^- \quad (4)$$

$$H_2O_2 + V_O\cdot \rightarrow OH- + \cdot OH \quad (5)$$

$$H_2O_2 + \cdot OH \rightarrow H_2O + \cdot OOH \quad (6)$$

$V_O\cdot$: the electron in SETOVs.

4 Conclusions

In this work, we have clearly identified the cause of the activity of the TiO_2-H_2O_2 system under dark conditions for the first time. TiO_2 NPs with SETOVs were prepared successfully and dispersed in water to form stable dispersion. Compared to TiO_2 or H_2O_2 alone, the composite catalyst exhibited super high catalytic activity on organics degradation in the dark. And the results indicate that H_2O_2 is activated by SETOVs existed in TiO_2 bulk phase. The transferring process of H_2O_2 into $\cdot O_2^-$/·OOH and ·OH are confirmed. In addition, both $\cdot O_2^-$/·OOH and ·OH were confirmed to indeed behave as effective active species for enhanced catalytic activity of TiO_2-H_2O_2 system. The present study provides new insight into the significant role of SETOVs in H_2O_2 activation in the dark. In comparison with most developed photocatalysis technologies, this strategy is much more energy-saving, and the application of TiO_2 in environmental protection could be widely broadened.

Acknowledgements

This work was supported by the National Natural Science Foundation of China (Nos. 21703046 and 21972028) and the Ministry of Science and Technology of China (No. 2016YFF0203803).

References

[1] O'Regan, B.; Grätzel, M. A low-cost, high-efficiency solar cell based on dye-sensitized colloidal TiO_2 films. *Nature* **1991**, *353*, 737–740.

[2] Fujishima, A.; Honda, K. Electrochemical photolysis of water at a semiconductor electrode. *Nature* **1972**, *238*, 37–38.

[3] Fujishima, A.; Zhang, X. T.; Tryk, D. A. TiO_2 photocatalysis and related surface phenomena. *Surf. Sci. Rep.* **2008**, *63*, 515–582.

[4] Chen, X. B.; Mao, S. S. Titanium dioxide nanomaterials: Synthesis, properties, modifications, and applications. *Chem. Rev.* **2007**, *107*, 2891–2959.

[5] Xie, Y. J.; Zhang, X.; Ma, P. J.; Wu, Z. J.; Piao, L. Y. Hierarchical TiO_2 photocatalysts with a one-dimensional heterojunction for improved photocatalytic activities. *Nano Res.* **2015**, *8*, 2092–2101.

[6] Wang, M.; Zhen, W. L.; Tian, B.; Ma, J. T.; Lu, G. X. The inhibition of hydrogen and oxygen recombination reaction by halogen atoms on over-all water splitting over Pt-TiO_2 photocatalyst. *Appl. Catal. B: Environ.* **2018**, *236*, 240–252.

[7] Li, X.; Shi, J. L.; Hao, H. M.; Lang, X. J. Visible light-induced selective oxidation of alcohols with air by dye-sensitized TiO_2 photocatalysis. *Appl. Catal. B: Environ.* **2018**, *232*, 260–267.

[8] Wu, Z. J.; Cao, S.; Zhang, C.; Piao, L. Y. Effects of bulk and surface defects on the photocatalytic performance of size-controlled TiO_2 nanoparticles. *Nanotechnology* **2017**, *28*, 275706.

[9] Zhang, Y.; Cui, W. Q.; An, W. J.; Liu, L.; Liang, Y. H.; Zhu, Y. F. Combination of photoelectrocatalysis and adsorption for removal of bisphenol A over TiO_2-graphene hydrogel with 3D network structure. *Appl. Catal. B: Environ.* **2018**, *221*, 36–46.

[10] Zhang, C.; Wu, Z. J.; Liu, J. J.; Piao, L. Y. Preparation of MoS_2/TiO_2 composite catalyst and its photocatalytic hydrogen production activity under UV irradiation. *Acta Phys.-Chim. Sin.* **2017**, *33*, 1492−1498.

[11] Wang, Y. Y.; Yang, W. J.; Chen, X. J.; Wang, J.; Zhu, Y. F. Photocatalytic activity enhancement of core-shell structure g-C_3N_4@TiO_2 via controlled ultrathin g-C_3N_4 layer. *Appl. Catal. B: Environ.* **2018**, *220*, 337–347.

[12] Schneider, J.; Matsuoka, M.; Takeuchi, M.; Zhang, J. L.; Horiuchi, Y.; Anpo, M.; Bahnemann, D. W. Understanding TiO_2 photocatalysis: Mechanisms and materials. *Chem. Rev.* **2014**, *114*, 9919–9986.

[13] Asahi, R.; Morikawa, T.; Ohwaki, T.; Aoki, K.; Taga, Y. Visible-light photocatalysis in nitrogen-doped titanium oxides. *Science* **2001**, *293*, 269–271.

[14] Wei, Z.; Liu, D.; Wei, W. Q.; Chen, X. J.; Han, Q.; Yao, W. Q.; Ma, X. G.; Zhu, Y. F. Ultrathin TiO_2(B) nanosheets as the inductive agent for transfrering H_2O_2 into superoxide radicals. *ACS Appl. Mater. Interfaces* **2017**, *9*, 15533–15540.

[15] Sánchez, L. D.; Taxt-Lamolle, S. F. M.; Hole, E. O.; Krivokapić, A.; Sagstuen, E.; Haugen, H. J. TiO_2 suspension exposed to H_2O_2 in ambient light or darkness: Degradation of methylene blue and EPR evidence for radical oxygen species. *Appl. Catal. B: Environ.* **2013**, *142–143*, 662–667.

[16] Randorn, C.; Wongnawa, S.; Boonsin, P. Bleaching of methylene blueS by hydrated titanium dioxide. *ScienceAsia* **2004**, *30*, 149–156.

[17] Zhang, A. Y.; Lin, T.; He, Y. Y.; Mou, Y. X. Heterogeneous activation of H_2O_2 by defect-engineered TiO_{2-x} single crystals for refractory pollutants degradation: A Fenton-like mechanism. *J. Hazard. Mater.* **2016**, *311*, 81–90.

[18] Wiedmer, D.; Sagstuen, E.; Welch, K.; Haugen, H. J.; Tiainen, H. Oxidative power of aqueous non-irradiated TiO_2 -H_2O_2 suspensions: Methylene blue degradation and the role of reactive oxygen species. *Appl. Catal. B: Environ.* **2016**, *198*, 9–15.

[19] Zhou, C. J.; Luo, J. J.; Chen, Q. Q.; Jiang, Y. Z.; Dong, X. P.; Cui, F. M. Titanate nanosheets as highly efficient non-light-driven catalysts for degradation of organic dyes. *Chem. Commun.* **2015**, *51*, 10847–10849.

[20] Li, J. L.; Zhang, M.; Guan, Z. J.; Li, Q. Y.; He, C. Q.; Yang, J. J. Synergistic effect of surface and bulk single-electron-trapped oxygen vacancy of TiO_2 in the photocatalytic reduction of CO_2. *Appl. Catal. B: Environ.* **2017**, *206*, 300–307.

[21] Li, L. D.; Yan, J. Q.; Wang, T.; Zhao, Z. J.; Zhang, J.; Gong, J. L.; Guan, N. J. Sub-10 nm rutile titanium dioxide nanoparticles for efficient visible-light-driven photocatalytic hydrogen production. *Nat. Commun.* **2015**, *6*, 5881.

[22] Yan, J. H.; Liu, P.; Ma, C. R.; Lin, Z. Y.; Yang, G. W. Plasmonic near-touching titanium oxide nanoparticles to realize solar energy harvesting and effective local heating. *Nanoscale* **2016**, *8*, 8826–8838.

[23] Guan, L.; Chen, X. B. Photoexcited charge transport and accumulation in anatase TiO_2. *ACS Appl. Energy Mater.* **2018**, *1*, 4313−4320.

[24] Cheng, X. L.; Hu, M.; Huang, R.; Jiang, J. S. HF-free synthesis of anatase TiO_2 nanosheets with largely exposed and clean {001} facets and their enhanced rate performance as anodes of lithium-ion battery. *ACS Appl. Mater. Interfaces* **2014**, *6*, 19176–19183.

[25] Wu, Q.; Liu, M.; Wu, Z. J.; Li, Y. L.; Piao, L. Y. Is photooxidation activity of {001} facets truly lower than that of {101} facets for anatase TiO_2 crystals? *J. Phys. Chem. C* **2012**, *116*, 26800–26804.

[26] Liu, S. W.; Yu, J. G.; Wang, W. G. Effects of annealing on the microstructures and photoactivity of fluorinated N-doped TiO_2. *Phys. Chem. Chem. Phys.* **2010**, *12*, 12308–12315.

[27] Liao, J. H.; Shi, L. Y.; Yuan, S.; Zhao, Y.; Fang, J. H. Solvothermal synthesis of TiO_2 nanocrystal colloids from peroxotitanate complex solution and their photocatalytic activities. *J. Phys. Chem. C* **2009**, *113*, 18778–18783.

[28] Han, E.; Vijayarangamuthu, K.; Youn, J. S.; Park, Y. K.; Jung, S. C.; Jeon, K. J. Degussa P25 TiO_2 modified with H_2O_2 under microwave treatment to enhance photocatalytic properties. *Catal. Today* **2018**, *303*, 305–312.

[29] Singh, G. P.; Shrestha, K. M.; Nepal, A.; Klabunde, K. J.; Sorensen, C. M. Graphene supported plasmonic photocatalyst for hydrogen evolution in photocatalytic water splitting. *Nanotechnology* **2014**, *25*, 265701.

[30] Tian, F.; Zhang, Y. P.; Zhang, J.; Pan, C. X. Raman spectroscopy: A new approach to measure the percentage of anatase TiO_2 exposed (001) facets. *J. Phys. Chem. C* **2012**, *116*, 7515–7519.

[31] Xia, T.; Zhang, C.; Oyler, N. A.; Chen, X. B. Hydrogenated TiO_2 nanocrystals: A novel microwave absorbing material. *Adv. Mater.* **2013**, *25*, 6905–6910.

[32] Zou, J.; Gao, J. C.; Xie, F. Y. An amorphous TiO2 sol sensitized with H2O2 with the enhancement of photocatalytic activity. *J. Alloys Compd.* **2010**, *497*, 420–427.

[33] Fu, D.; Huang, Y. J.; Zhang, X. T.; Kurniawan, T. A.; Ouyang, T. Uncovering potentials of integrated TiO_2(B) nanosheets and H_2O_2 for removal of tetracycline from aqueous solution. *J. Mol. Liq.* **2017**, *248*, 112–120.

[34] Chen, J.; Ding, Z. Y.; Wang, C.; Hou, H. S.; Zhang, Y.; Wang, C. W.; Zou, G. Q.; Ji, X. B. Black anatase titania with ultrafast sodium-storage performances stimulated by oxygen vacancies. *ACS Appl. Mater. Interfaces* **2016**, *8*, 9142–9151.

[35] Liu, W.; Liu, H. C.; Ai, Z. H. *In-situ* generated H_2O_2 induced efficient visible light photo-electrochemical catalytic oxidation of PCP-Na with TiO_2. *J. Hazard. Mater.* **2015**, *288*, 97–103.

[36] Chen, X. B.; Liu, L.; Yu, P. Y.; Mao, S. S. Increasing solar absorption for photocatalysis with black hydrogenated titanium dioxide nanocrystals. *Science* **2011**, *318*, 746–750.

[37] Pan, X. Y.; Yang, M. Q.; Fu, X. Z.; Zhang, N.; Xu, Y. J. Defective TiO_2 with oxygen vacancies: Synthesis, properties and photocatalytic applications. *Nanoscale* **2013**, *5*, 3601–3614.

[38] Dong, G. Y.; Wang, X.; Chen, Z. W.; Lu, Z. Y. Enhanced photocatalytic activity of vacuum-activated TiO_2 induced by oxygen vacancies. *Photochem. Photobiol.*, **2018**, *94*, 472–483.

[39] Zeng, L.; Song, W. L.; Li, M. H.; Zeng, D. W.; Xie, C. S. Catalytic oxidation of formaldehyde on surface of H-TiO_2/H-C-TiO_2 without light illumination at room temperature. *Appl. Catal. B: Environ.* **2014**, *147*, 490–498.

[40] Hou, L. L.; Zhang, M.; Guan, Z. J.; Li, Q. Y.; Yang, J. J. Effect of annealing ambience on the formation of surface/bulk oxygen vacancies in TiO_2 for photocatalytic hydrogen evolution. *Appl. Surf. Sci.* **2018**, *428*, 640–647.

[41] Occhiuzzi, M.; Cordischi, D.; De Rossi, S.; Ferraris, G.; Gazzoli, D.; Valigi, M. Pd-promoted WO_x/ZrO_2 catalysts: Characterization and catalytic activity for *n*-butane isomerization. *Appl. Catal. A: General* **2008**, *351*, 29–35.

[42] Bedilo, A. F.; Plotnikov, M. A.; Mezentseva, N. V.; Volodin, A. M.; Zhidomirov, G. M.; Rybkin, I. M.; Klabunde, K. J. Superoxide radical anions on the surface of zirconia and sulfated zirconia: Formation mechanisms, properties and structure. *Phys. Chem. Chem. Phys.* **2005**, *7*, 3059–3069.

[43] Wang, J. J.; Li, Z. J.; Li, X. B.; Fan, X. B.; Meng, Q. Y.; Yu, S.; Li, C. B.; Li, J. X.; Tung, C. H.; Wu, L. Z. Photocatalytic hydrogen evolution from glycerol and water over nickel-hybrid cadmium sulfide quantum dots under visible-light irradiation. *ChemSusChem* **2014**, *7*, 1468–1475.

[44] Green, M. A.; Xu, J. L.; Liu, H. L.; Zhao, J. Y.; Li, K. X.; Liu, L.; Qin, H.; Zhu, Y. M.; Shen D. Z.; Chen, X. B. Terahertz absorption of hydrogenated TiO_2 nanoparticles. *Mater. Today Phys.* **2018**, *4*, 64–69.

[45] Green, M.; Liu, Z. Q.; Xiang, P.; Liu, Y.; Zhou, M. J.; Tan, X. Y.; Huang, F. Q.; Liu, L.; Chen, X. B. Doped, conductive SiO_2 nanoparticles for large microwave absorption. *Light: Sci. Appl.* **2018**, *7*, 87.

[46] Wang, Y.; Meng, X. J.; Yu, X. L.; Zhang, M.; Yang, J. J. Recoverable visible light photocatalytic activity of wide band gap nanotubular titanic acid induced by H_2O_2-pretreatment. *Appl. Catal. B: Environ.* **2013**, *138–139*, 326–332.

[47] Pi, L.; Yang, N.; Han, W.; Xiao, W.; Wang, D. H.; Xiong, Y.; Zhou, M.; Hou, H. B.; Mao, X. H. Heterogeneous activation of peroxymonocarbonate by Co-Mn oxides for the efficient degradation of chlorophenols in the presence of a naturally occurring level of bicarbonate. *Chem. Eng. J.* **2018**, *334*, 1297–1308.